Physics Letters B 748 (2015) 306–310

Contents lists available at ScienceDirect

Physics Letters B

www.elsevier.com/locate/physletb

Magnetic guidance of charged particles

Dirk Dubbers

Physikalisches Institut der Universität, Im Neuenheimer Feld 226, 69120 Heidelberg, Germany

ARTICLE INFO

Article history:
Received 22 January 2015
Received in revised form 18 May 2015
Accepted 2 July 2015
Available online 3 July 2015
Editor: V. Metag

Keywords:
Leptonic, semileptonic, and radiative decays
Nuclear tests of fundamental interactions and symmetries
Charged-particle spectroscopy
Magneto-optical devices
Neutrons, neutrinos

ABSTRACT

Many experiments and devices in physics use static magnetic fields to guide charged particles from a source onto a detector, and we ask the innocent question: What is the distribution of particle intensity over the detector surface? One should think that the solution to this seemingly simple problem is well known. We show that, even for uniform guide fields, this is not the case, and we present analytical point spread functions (PSF) for magnetic transport that deviate strongly from previous results. The "magnetic" PSF shows unexpected singularities, which were recently also observed experimentally, and which make detector response very sensitive to minute changes of position, field amplitude, or particle energy. In the field of low-energy particle physics, these singularities may become a source of error in modern high precision experiments, or may be used for instrument tests.

1. Introduction

The motion of charged particles in magnetic fields is a highly developed subject, treated in numerous papers and books. The most frequently investigated case is magnetic focusing, as used in electron microscopes, oscilloscopes, electron spectrometers, particle accelerators, or in mass spectrometers with magnetic sector fields. Electron optics was developed early in the past century [1], mainly for small angular ranges of particle emission $\Delta\theta \ll 1$, and for trajectories that describe less than one full orbit of gyration ($n < 1$), see also [2] and the books quoted therein. The case of a magnetic β-ray spectrometer based on one full orbit ($n = 1$) was treated in [3,4], while a survey on magnetic electron and ion spectrometers is given in [5].

In more recent times, magnetic fields are increasingly being used to simply guide charged particles, like electrons, muons, ions, or other, efficiently from a source to a detector. Such setups are found in magnetic photoelectron imaging [6–8], invented in the early 1980s, molecular reaction microscopes [9,10] (early nineties), retardation spectrometers [11–13] (early nineties), time projection chambers [14] (mid-seventies), or in muon [15], neutron [16,17], or nuclear decay spectrometers [18], to name just a few experiments and surveys. In these applications, charged particles are emitted over a wide range of emission angles ($0 < \theta \leq \pi/2$), and the number of orbits of gyration may vary widely ($0 < n < \infty$). This magnetic guidance of charged particle is the topic of the present paper.

For particles emitted from a *point* source, the distribution function of particle intensity over the detector plane is called a point spread function (PSF). Once a PSF is known, the particle distribution for any type of extended source can be calculated from it. One should think that the magnetic PSF for this setup is well known and no longer subject of investigation. But this is not the case, and we find some striking features in this PSF which, to our knowledge, have not been published before, and which may be of interest to a wider community.

Our particular interest is on the role of the magnetic PSF in the field of low-energy particle physics, which field is entering what some call the high-precision era [19–21], often searching for 10^{-4} effects that might signal new physics beyond the standard model, at a level where Monte Carlo simulations often meet difficulties. In a recent publication [22] we had sketched the derivation of the PSF and its singularities in the context of neutron β-decay, and had listed over a dozen neutron decay experiments that use magnetic guiding of charged reaction products for high precision measurements.

The present paper shows how the predicted strong singularities, absent in the conventional treatment of the PSF, appear in the true PSF. Some of these singularities move rapidly across the PSF when the minimum number n_0 of gyration orbits is changed by only a small fraction of one orbit. These singularities make detector response very sensitive to minute changes of instrumental parameters like field amplitude, particle energy, and detector position

E-mail address: dubbers@physi.uni-heidelberg.de.

http://dx.doi.org/10.1016/j.physletb.2015.07.004

or angular adjustment. We then extend calculations to anisotropic sources and non-uniform guide fields. We sketch a recent experiment [23] done at LANL, in which the resonances predicted in [22] were observed, and discuss some possible uses of the true magnetic PSF.

2. The conventional magnetic point spread function (PSF)

Let a point source of charged particles be placed at position $\boldsymbol{x} = 0$ in a uniform magnetic field of amplitude B, applied along axis z. Let the particles on their helical trajectories be intercepted by a flat detector installed in the x–y plane at distance z_0 to the source. We first sketch the conventional approach to the problem, which leads to a smooth PSF, used already some 30 years ago [7], and still in use up to these days [8].

Without loss of generality, let the charged particles be monoenergetic electrons. Their radius of gyration r depends on their polar angle of emission θ as

$$r = r_0 \sin\theta, \tag{1}$$

and on their kinetic energy E via the maximum radius of gyration as

$$r_0 = p/eB = \sqrt{E\left(E + 2mc^2\right)}/ecB, \tag{2}$$

with electron charge e, mass m, and relativistic momentum p. We assume a uniform magnetic field, for the non-uniform case see Section 5. The pitch of the helix is $d = 2\pi r_0 \cos\theta$. These formulas are found in most textbooks on electromagnetism.

Upon arrival of an electron on the detector, its total number of gyration orbits is $n' = z_0/d$, where the slash reminds us that n' needs not be an integer. The total phase angle of gyration is hence related to the angle of electron emission θ as

$$\alpha = 2\pi n' = z_0/(r_0 \cos\theta). \tag{3}$$

The smallest occurring phase angle, reached for electron emission under $\theta = 0$, is

$$\alpha_0 = z_0/r_0 = 2\pi n_0, \quad \text{where} \tag{4}$$

$$n_0 = eBz_0/2\pi p \tag{5}$$

is the corresponding minimum number of orbits in the limit $\theta \to 0$ (where in fact a gyration is no longer visible). On the detector, the electron's point of impact is displaced from its projected starting point, reached for $\theta = 0$, by the distance

$$R = 2r|\sin\alpha/2| = 2r_0 \sin\theta \sin\alpha/2', \tag{6}$$

where $\alpha' = (\alpha \text{ modulo } 2\pi)$ is the phase angle seen on the surface of the detector, with $0 \le \alpha' \le 2\pi$.

The conventional approach to the problem is to assume that all phase angles occur with the same probability, see [23] for a straightforward derivation of the magnetic PSF under this assumption. In this approach, the probability $\mathrm{d}P/\mathrm{d}R$ for finding an electron at displacement R no longer depends on R,

$$g(R) \equiv \frac{\mathrm{d}P}{\mathrm{d}R} = \frac{1}{2r_0}. \tag{7}$$

An intermediate result in the derivation of $g(R)$, needed below in Section 5, is the distribution

$$\left|\frac{\mathrm{d}g}{\mathrm{d}\cos\theta}\right| = \frac{2}{\pi\sqrt{4r_0^2 \sin^2\theta - R^2}} \tag{8}$$

with respect to the polar emission angle θ at the source.

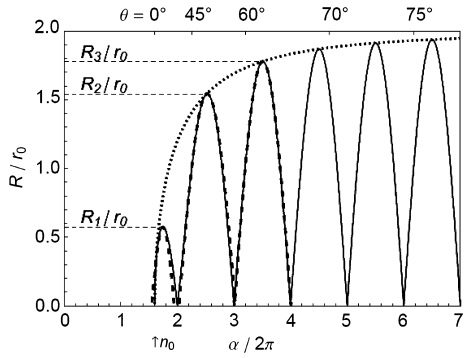

Fig. 1. Electron displacement R on the detector from Eq. (11), plotted as a function of the number of orbits $n' = \alpha/2\pi$ (full line). The corresponding angles of emission θ from Eq. (3) are given on the upper axis. The envelope function $2r_0 \sin\theta(\alpha)$ in Eq. (6) is also shown (dotted line). The value $\alpha_0 = 10$ radians, or $n_0 = \alpha_0/2\pi = 1.6$ orbits, is the same as in the experiment [23], in which $B \sim 1/2$ T, $z_0 \sim 0.1$ m, and $E \sim 1$ MeV, see Section 6. The dashed lines are the invertible approximations to $R(\alpha)$ from Eqs. (15) and (22).

For given R and $\mathrm{d}R$, the electrons arrive on the detector within an infinitesimal area of size $\mathrm{d}A = 2\pi R\mathrm{d}R$. The radially symmetric PSF $f(x, y) = f(R)$, with $R = (x^2 + y^2)^{1/2}$ on the detector surface, then is the hyperbolic function

$$f(R) \equiv \frac{\mathrm{d}P}{\mathrm{d}A} = \frac{g(R)}{2\pi R} = \frac{1}{4\pi R r_0}. \tag{9}$$

The singularity at $R = 0$ reflects the fact that all orbits cross the origin, for arbitrary values of emission angles θ and φ, and of energy E. Fig. 2 of [24] shows a rough measurement of such an $1/R$ response. Note that in [22] we inadvertently called the function $g(R)$ the PSF, and not the function $f(R)$.

However, this conventional result cannot be the full truth, because, in its derivation from Eq. (6), the phase angle α and the pitch angle θ were treated as independent variables. In other words: for a given emission angle θ, the electron on the detector is erroneously assumed to run on a circle through all values of α.

3. Derivation of the true magnetic PSF

In reality, both angles α and θ are uniquely linked to each other by Eqs. (3) and (4) as

$$\cos\theta = \alpha_0/\alpha. \tag{10}$$

After emission under θ, the electron hence arrives at one fixed and predetermined position on the detector, given by the electron displacement

$$R(\alpha) = 2r_0\sqrt{1 - \alpha_0^2/\alpha^2}\,|\sin\alpha/2|, \tag{11}$$

from Eq. (6). To increase the size of the phase angle α on the detector, one has to increase the emission angle θ at the source, and with it the gyration radius r from Eq. (1), such that the trace on the detector is no longer a circle but some sort of a spiral.

Fig. 1 shows R in dependence of the total number of electron orbits $n' = \alpha/2\pi$. The function starts at the minimum number of orbits $n_0 = \alpha_0/2\pi$ for emission under $\theta = 0$, and continues, with increasing emission angle θ, to $\alpha/2\pi \to \infty$ for emission under $\theta = \pi/2$. One could as well write R as a function of emission angle θ, with the same final result for the PSF. However, while θ is the more directly accessible variable, the derivation is simpler in terms of the variable α.

We now come to the calculation of the true PSF. Often the polar angular distribution of the particles emitted from a source is

developed in Legendre polynomials as functions of $\cos\theta$. Therefore the PSF is best written as

$$f(R) = \frac{1}{2\pi R}\left|\frac{dP}{d\cos\theta}\frac{d\cos\theta}{d\alpha}\frac{d\alpha}{dR}\right|. \tag{12}$$

We first treat the isotropic case $dP/d\cos\theta = 1$, for anisotropic sources see Section 5. Insertion of $d\cos\theta/d\alpha$ from Eq. (3) and of $(dR/d\alpha)^{-1}$ from Eq. (11) then leads to

$$f(\alpha) = \frac{1}{2\pi R r_0}\frac{\alpha_0(\alpha^2-\alpha_0^2)^{1/2}}{|\alpha(\alpha^2-\alpha_0^2)\cos\alpha/2 + 2\alpha_0^2\sin\alpha/2|}. \tag{13}$$

However, we need the PSF not as a function of α, but as a function of R. Inversion of the multi-valued function $R(\alpha)$ of Fig. 1 to $\alpha(R)$ is the main obstacle to arriving at the true magnetic PSF.

While Eq. (13) is still exact, we now use the fact that the displacement $R(\alpha)$, Eq. (11), is the product of a rapidly varying function $|\sin(\alpha/2)|$ and a slowly varying envelope $2r_0(1-\alpha_0^2/\alpha^2)^{1/2}$, as seen in the example of Fig. 1. Within a given cycle on the detector, numbered by the integer n, the slow envelope can therefore be piecewise approximated by a constant value R_n, which is best chosen to be the maximum of $R(\alpha)$ in the nth interval,

$$R_n = \mathrm{Max}[R(\alpha), 2\pi n \le \alpha \le 2\pi(n+1)], \tag{14}$$

as indicated by the dashed horizontal lines in Fig. 1. The true function $R(\alpha)$ from Eq. (11) then is piecewise replaced by the approximate functions

$$R(\alpha) \approx R_n\cos[(\alpha-\alpha'_n)/2], \tag{15}$$

where α'_n is the position where $R(\alpha)$ obtains its maximum R_n, each valid between $\alpha = 2\pi n$ and $\alpha = 2\pi(n+1)$. Note that for the lowest orbit starting at n_0, these equations hold only for integer n_0, for non-integer n_0 see below.

The dashed curves in Fig. 1 show these invertible functions Eq. (15), indicating the high quality of the approximation. For each orbit, the approximate $R(\alpha)$ can be resolved for α,

$$\alpha_\pm(R) \approx \alpha'_n \mp 2\arccos(R/R_n), \tag{16}$$

where α_+ holds for the *rising* branches of $R(\alpha)$ in Fig. 1, and α_- for the *falling* branches.

These approximate α's then must be inserted in Eq. (13). In this way one obtains for every cycle a partial PSF that we call f_n. These partial PSFs must then be summed up to obtain the magnetic PSF,

$$f(R) \approx \sum_{n=n_0}^{\infty} f_n(R). \tag{17}$$

For integer n_0, one finds in the denominator of Eq. (13)

$$\cos(\alpha/2) \approx \pm\sqrt{1-R^2/R_n^2}, \qquad \sin(\alpha/2) \approx R/R_n, \tag{18}$$

with the plus sign for the rising branches, the minus sign for the falling branches. After Eqs. (18) are inserted in Eq. (13), one can, for not too small values of n_0, neglect $2\arcsin(R/R_n)$ in Eq. (16) for the other α's and set $\alpha_n = 2\pi n$. The nth partial PSF for an isotropic source in a uniform magnetic field then reads

$$f_n(R) \approx f_{n+}(R) + f_{n-}(R), \quad \text{with} \tag{19}$$

$$f_{n\pm}(R) = \frac{1}{4\pi R r_0}\frac{n_0(n^2-n_0^2)^{1/2}}{|\pm\pi n(n^2-n_0^2)(1-R^2/R_n^2)^{1/2} + n_0^2 R/R_n|}. \tag{20}$$

Usually n_0 is not an integer, in which case special attention must be given to the lowest orbit, then numbered by the next-lower integer $n_f = \mathrm{floor}(n_0)$. The width of the lowest interval in Fig. 1 then is less than unity, namely, $2 - 1.6 = 0.4$. This requires replacing Eq. (14) by

$$R_{n_f} = \mathrm{Max}[R(\alpha), 2\pi n_0 \le \alpha \le 2\pi(n_f+1)], \tag{21}$$

and Eq. (15) by

$$R(\alpha) \approx R_{n_f}\left|\cos\frac{\alpha-\alpha'_{n_f}}{2(n_f+1-n_0)}\right|, \tag{22}$$

valid between $\alpha = 2\pi n_0$ and $\alpha = 2\pi(n_f+1)$, where α'_{n_f} is the position where $R(\alpha)$ has its first maximum R_{n_f}. This can be resolved for α as

$$\alpha_\pm(R) \approx \alpha'_{n_f} \mp 2(n_f+1-n_0)\arccos(R/R_{n_f}). \tag{23}$$

Used in Eq. (13), this gives the first partial PSF $f_{n_f}(R)$, and the sum Eq. (17) starts at $n = n_f$.

At the start of the lowest orbit where α is near α_0, it is useful to replace Eq. (23) by the approximate inverted function $\alpha_+(R) \approx \alpha_0[1 + R^2/(8\sin^2\alpha/2)]$. In Fig. 2b this is done up to $R = 0.34$. In Figs. 2a and 3 this replacement would avoid the little kinks seen at low R. Finally, the normalization of $g(R)$ to unity was checked by numerical integration of $g(R)$, taken from the general Eq. (17).

4. Properties of the magnetic PSF

Fig. 2a shows the new PSF $f(x,y)$, calculated directly from Eq. (13) with (16) and (23) for $n_0 = 1.6$. Strong resonances are seen whenever R falls onto one of the maxima R_n in Fig. 1. Summation of the f_n is truncated at $n_2 = 50$. With $\cos\theta = n_0/n$ from Eq. (10), this corresponds to a cut off angle $\theta = 88.2°$, with no visible effect to the PSF in Fig. 2a. Fig. 2b shows $g(R) = 2\pi R f(R)$, both for the conventional and the new approach.

The positions and shapes of the resonances can be understood by looking at $R(\alpha)$ in Fig. 1. The fluctuating $R(\alpha)$ and its smooth envelope $|\sin\theta(\alpha)|$ coincide near each maximum R_n. This means that α and θ in Eq. (6) are strongly correlated there, contrary to the conventional assumption of independence of α and θ. Therefore the deviations of the true PSF from the conventional PSF are strongest at $R \approx R_n$. They are singular because the derivative $d\alpha/dR$ in Eq. (12) diverges whenever $R(\alpha)$ reaches a maximum R_n near a half-integer number of revolutions, where $R(\alpha)$ becomes stationary. If R is increased above a particular R_n, the correlation between α and θ in the corresponding orbit is suddenly lost, cf. Fig. 1, and only the rather uncorrelated terms from the higher orbits contribute to Eq. (17). Therefore the true PSF descends steeply whenever R rises beyond one of the R_n.

In terms of emission angle θ, the ring-shaped singularities in Fig. 2 occur at $\theta_1 = 27.6°$, $\theta_2 = 50.5°$, $\theta_3 = 63.0°$, etc., from Eqs. (21) and (14) with Eq. (6). For large integer $n_0 \gg 1$, the first few singularities of the PSF occur for emission angles and displacements

$$\theta_n \approx \sqrt{2(n-n_0)/n_0}, \qquad R_n \approx 2r_0\sqrt{[2(n-n_0)+1]/n_0}. \tag{24}$$

Fig. 3 demonstrates the high sensitivity of the true PSF to changes of external parameters that define the minimum number of orbits n_0, cf. Eq. (5). Note that in Fig. 3, n_0 is ten times larger than in Figs. 1 or 2. The sensitivity of the PSF to changes of n_0 can again be understood by looking at the corresponding changes of R in Fig. 1. For instance, when an integer n_0 changes continuously to the next higher integer $n_0 + 1$, then the first maximum moves

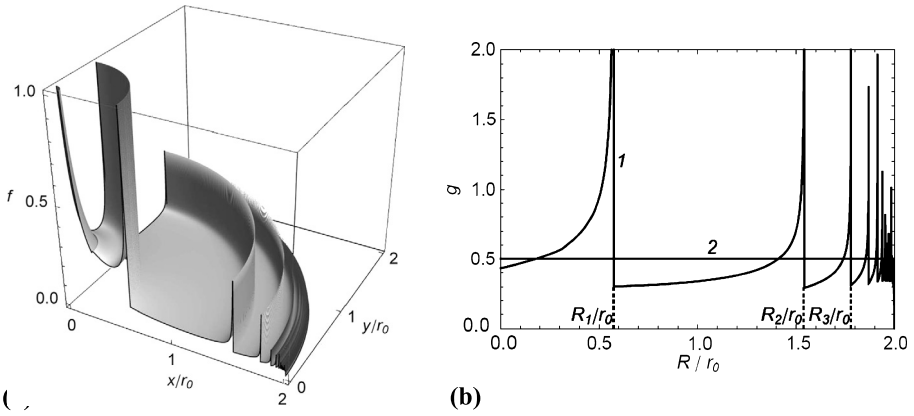

Fig. 2. (a) Magnetic point spread functions $f(x, y)$ from Eq. (13) with (16) and (23), in the first quadrant of the detector, for isotropic particle emission and uniform field. The same $\alpha_0 = 10$ radians, or $n_0 = 1.6$ orbits, are used as in Fig. 1. **(b)** The spiked function labeled 1 is the new probability distribution $g(R) = 2\pi R f(R)$. The constant function labeled 2 is the conventional distribution $g(R) = 1/(2r_0)$. The positions of the resonances (dashed vertical lines) coincide with the corresponding maxima R_n in Fig. 1.

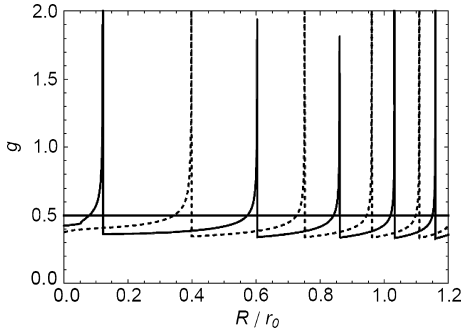

Fig. 3. Sensitivity of the probability distributions $g(R) = 2\pi R f(R)$ to changes of the external parameters, cf. Eq. (5). While the conventional distribution (horizontal line) does not depend on external parameters, the true distribution is highly parameter dependent. The full curve is for $\alpha_0 = 105$ radians, or $n_0 = 16.7$ orbits, the dashed curve for a 3% lower value $\alpha_0 = 102$ radians, or $n_0 = 16.2$ orbits. Only the first half of the allowed R/r_0 interval is shown.

from zero to its peak value (which is $R_1 = 0.73r_0$ for the interval from $n_0 = 1$ to $n_0 = 2$), and back to zero again. At the same time, relative intensities and widths of the resonances may vary considerably.

This parameter sensitivity of n_0 may average out the singularities of the PSF: These singularities are no longer individually resolved experimentally if n_0 changes by $\Delta n_0 > 1$. This happens when either $\Delta B/B$ (e.g., for extended sources), or $\Delta z_0/z_0$ (for axially extended sources), or $|\Delta p/p|$ (for continuous spectra) in Eq. (5) exceeds $1/n_0$. Note that often Δn_0 can be kept small by additional time-of-flight measurements and energy sensitive detection.

5. Anisotropic sources and non-uniform guide fields

This section treats two extensions of our analytic PSF calculations. The first extension is to non-isotropic sources. Often the polar angular distribution $\mathrm{d}P/\mathrm{d}\cos\theta$ in Eq. (12) can be developed in associated Legendre polynomials, involving terms

$$\frac{\mathrm{d}P}{\mathrm{d}\cos\theta} \sim \cos^{l-m}\theta \sin^m\theta, \tag{25}$$

with integer $m \le l$. An example is particle emission from atoms or nuclei that carry a vector or tensor polarization, see for instance Chapters 19.3 and 20.5 in [25].

We begin with the conventional PSFs for anisotropic sources. If variations of Δn_0 are so large as to average out the singularities in the PSF, we can insert the distribution (25) into the integrand Eq. (8). The conventional PSF for anisotropic sources then is

$$f_m^l(R) = g_m^l(R)/2\pi R, \quad \text{with} \tag{26}$$

$$g_m^l(R) = (1/r_0)\left[1 - R^2/4r_0^2\right]^{(l-m)/2} \times {}_2F_1\left(-m/2, (l-m+1)/2; (l-m+2)/2; 1 - R^2/4r_0^2\right), \tag{27}$$

with the hypergeometric function ${}_2F_1$. For the normalization of this function to $g_m^l(0) = 1$, see the preprint [26].

For $m = 0$, which involves only ordinary Legendre polynomials with terms $\cos^l\theta$, one finds $g_0^l(R) = (1 - R^2/4r_0^2)^{l/2}/2r_0$. For $l = 0$ this coincides with the result (7) for isotropic sources. For $l = 1$ this last equation gives the PSFs for angular correlation functions, like the parity violating β asymmetry, see [22] for details, and again [26] for further examples.

To obtain the true PSF for anisotropic sources, we insert $\cos\theta = n_0/n$ into Eq. (25) and multiply each partial PSF in the sum (17) by the resulting $(n_0/n)^{l-m}[1 - (n_0/n)^2]^{m/2}$. This gives the true PSFs $f_m^l(R)$, which again show singularities for every $R = R_n$. When these singularities are averaged out, the corresponding conventional solution from Eq. (27) is recovered.

Our second extension treats the case that the magnetic field, while still axially symmetric, is not uniform. In many experiments the field decreases continuously from B at the source to B' at the detector, which avoids glancing incidence on the detector for particles emitted near $\theta = \pi/2$. In the experiments [3–18] cited in the introduction, non-adiabatic transitions are strictly suppressed because their angle dependent energy losses would corrupt the measurements. In the adiabatic approximation, for $B' < B$ the inverse magnetic mirror effect makes the gyration radius widen from r at the source to $r' = r/(B'/B)^{1/2}$ on the detector, while the pitch angle decreases from θ to θ', with $\sin\theta' = (B'/B)^{1/2}\sin\theta$.

We expect that the usual adiabatic invariants, on which these equations are based, guarantee that the overall particle distribution on the detector remains unchanged, stretched, however, by a factor $(B/B')^{1/2}$. Although this conjecture sounds reasonable, we checked it analytically in [26] and found that the PSFs for a uniform ($B = B'$) and for a non-uniform field ($B \neq B'$) indeed are related as $f'(R') = f(R\sqrt{B'/B})$.

6. Experimental verification, and possible applications of the new PSF

A recent experiment [23], done at the Los Alamos National Laboratory on the ultracold neutron decay spectrometer UCNA [27], has meanwhile confirmed the predicted presence of resonances in the true PSF. In this work, an isotropic ^{207}Bi conversion electron source ($E = 976$ keV and 432 keV) in a uniform magnetic guide field was placed at 10 cm distance to a position sensitive Si detector of 10 cm diameter and 0.8 cm^2 pixel size. The field amplitude B then was varied between 0.1 and 0.6 T, thus varying r_0 from 4.0 cm down to 0.7 cm. Every time one of the resonances of the PSF from Fig. 2a entered or left a pixel, there was a sudden jump in the count rate from this pixel. Small changes of the magnetic field induced large changes in relative count rates (up to a factor of five), see Figs. 7 and 8 in [23], where the conventional PSF would predict a very smooth response. The agreement with simulated expectations is excellent. The Monte Carlo result in their Fig. 4 can be compared to our result in Fig. 2b, calculated with identical parameters, namely, $n_0 = 1.6$. Note that our resonances are narrower and steeper than the Monte Carlo result from [23]. Hence care must be taken when applying these calculations to possibly inherently broadened experimental data.

What are the possible benefits of having a new PSF? First, knowledge on the ring-shaped singularities in the PSF may promote understanding of experimental data and avoid surprises, for instance in reaction microscopy or similar experiments. Second, even when these rings remain unresolved, one must investigate their effect in high precision experiments, as was done for neutron decay in [22,23]. Third, these rings may serve as an analytical tool to assess the proper working of magnetic guiding systems.

As an example for this last point, we take the retardation spectrometer of the neutrino mass experiment KATRIN [13]. Its length from the effective ^{3}H source to the electron detector is $z_0 = 51.8$ m. Although KATRIN's minimum field is well below 1 mT, its relevant average field is $\bar{B}_z = 1$ T, as deduced from [28]. For the 976 keV conversion line of a ^{207}Bi test source, installed on-axis at the entrance of the spectrometer, Eq. (5) gives $n_0 = 2000$ orbits to the detector, all fully contained in the detector volume. Each conversion electron crosses the instrument axis at every cycle of gyration. KATRIN's ring-shaped electron detector, installed at the end of the instrument, can then measure the resulting PSF to check whether it is properly shaped. The Bi-source should be installed somewhat upstream of the initial field maximum to limit $\theta_{\max}$, and the detector should be moved further downstream of the pitch field region to adapt gyration radii to detector size. In this way the entire spectrometer volume could be probed for possible discrepancies. These thoughts serve merely to remind the reader that new insights may generate new opportunities.[1] Similar studies could be done on the neutron decay spectrometers PERC [29] with $n_0 = 200$, Nab [30] with $n_0 = 170$, or Perkeo-III [31] with $n_0 = 15$. Note added: A recent preprint [32] combines our initial approach with a special numerical method and finds results that coincide precisely with our result in Fig. 2b. The discrepancies mentioned in this paper refer to the first version of our preprint [26] where a less precise approximation had been used.

7. Conclusions

We calculated the point spread functions for charged particles in magnetic guide fields, which differ significantly from previously used results, as seen in Fig. 2b. Algebraic results are derived for isotropic and anisotropic point sources, for uniform and non-uniform guide fields, valid also for sources rather close to the detector. The singularities found move rapidly across the PSF when the number of gyration orbits is changed by as little as a fraction of one orbit, see Fig. 3. A recent experiment done at LANL corroborates these results.

Acknowledgements

This work was supported by the Priority Programme SPP 1491 of Deutsche Forschungsgemeinschaft. I thank L. Raffelt, B. Märkisch, F. Friedl, and H. Abele for helpful discussions on the applications of magnetic PSFs in neutron decay.

References

[1] H. Busch, Ann. Phys. (Leipz.) 386 (1926) 974.
[2] V. Kumar, Am. J. Phys. 77 (2009) 737.
[3] C.M. Witcher, Phys. Rev. 60 (1941) 32.
[4] J.W.M. Dumond, Ann. Phys. 2 (1957) 283.
[5] K. Siegbahn (Ed.), Alpha-, Beta- and Gamma-Ray Spectroscopy, Elsevier, Amsterdam, 1955, p. 52.
[6] G. Beamson, H.Q. Porter, D.W. Turner, Nature 290 (1981) 556.
[7] P. Kruit, F.H. Read, J. Phys. E 16 (1983) 313.
[8] R. Browning, Rev. Sci. Instrum. 85 (2014) 033705.
[9] R. Moshammer, et al., Phys. Rev. Lett. 73 (1994) 3371.
[10] J. Ullrich, et al., Rep. Prog. Phys. 66 (2003) 1463.
[11] G. Drexlin, et al., Adv. High Energy Phys. 2013 (2013) 293986.
[12] V.N. Aseev, et al., Phys. Rev. D 84 (2011) 112003.
[13] E.W. Otten, C. Weinheimer, Rep. Prog. Phys. 71 (2008) 086201.
[14] J.N. Marx, D.R. Nygren, Phys. Today 31 (1978) 10.
[15] J. Kaulard, et al., Phys. Lett. B 422 (1998) 334.
[16] H. Abele, Prog. Part. Nucl. Phys. 60 (2008) 1.
[17] D. Dubbers, M.G. Schmidt, Rev. Mod. Phys. 83 (2011) 1111.
[18] M. Beck, et al., Eur. Phys. J. A 47 (2011) 45.
[19] K. Blaum, H. Müller, N. Severijns, Ann. Phys. (Leipz.) 525 (2013) A111.
[20] V. Cirigliano, S. Gardner, B. Holstein, Prog. Part. Nucl. Phys. 71 (2013) 93.
[21] A.S. Kronfeld, R.S. Tschirhart (Eds.), U. Al-Binni, et al., arXiv:1306.5009 [hep-ex].
[22] D. Dubbers, et al., Nucl. Instrum. Methods Phys. Res., Sect. A, Accel. Spectrom. Detect. Assoc. Equip. 763 (2014) 112.
[23] S.K.L. Sjue, et al., Rev. Sci. Instrum. 86 (2015) 023102.
[24] H. Kollmus, et al., Nucl. Instrum. Methods Phys. Res., Sect. B, Beam Interact. Mater. Atoms 124 (1997) 377.
[25] D. Dubbers, H.-J. Stöckmann, Quantum Physics: The Bottom-Up Approach – From the Simple Two-Level System to Irreducible Representations, Springer, Heidelberg, 2013.
[26] D. Dubbers, arXiv:1501.05131v2 [physics.ins-det].
[27] M.P. Mendenhall, et al., Phys. Rev. C 87 (2013) 032501.
[28] F. Glück, et al., New J. Phys. 15 (2013) 083025.
[29] D. Dubbers, et al., Nucl. Instrum. Methods Phys. Res., Sect. A, Accel. Spectrom. Detect. Assoc. Equip. 596 (2008) 238.
[30] S. Baeßler, et al., arXiv:1209.4663 [nucl-ex].
[31] B. Märkisch, et al., Nucl. Instrum. Methods Phys. Res., Sect. A, Accel. Spectrom. Detect. Assoc. Equip. 611 (2009) 216.
[32] H. Backe, arXiv:1503.07064v1 [physics.ins-det].

[1] In the meantime I learned from C. Weinheimer that at 976 keV, adiabatic transport is no longer guaranteed in the KATRIN spectrometer.